(Received 13 December 2023, Accepted 2 January 2024, Scheduled 15 January 2024)

A Quad Port MIMO Antenna Using Rectangular Dielectric Resonator Antenna Array for Intelligent Transportation System Applications

Goffar Ali Sarkar[1, 2, *], Khan Masood Parvez[3], Arunachalam Ambika[4], Tanvir Islam[5], Sudipta Das[6], Utpal Mandal[2], and Susanta Kumar Parui[1]

[1]*Department of Electronics and Telecommunication Engineering, Indian Institute of Engineering Science and Technology, Shibpur, Howrah-711103, WB, India*
[2]*Department of Electronics and Telecommunication Engineering, Kalimpong Government Polytechnic, Kalimpong-734301, India*
[3]*Department of Electronics and Communication Engineering, Aliah University, Kolkata-700156, India*
[4]*Department of Electronics and Communication Engineering, B.S. Abdur Rahman Crescent Institute of Science and Technology, Tamil Nadu 600048, India*
[5]*Department of Electrical and Computer Engineering, University of Houston, Houston, TX 77204, USA*
[6]*Department of Electronics and Communication Engineering, IMPS College of Engineering and Technology, Malda-732103, West Bengal, India*

ABSTRACT: This article presents a quad port multi-input multi-output (MIMO) antenna based on arrays of rectangular dielectric resonators for intelligent automotive applications. The proposed MIMO antenna configuration is formulated by integrating four rectangular dielectric resonator antenna (RDRA) arrays. Two RDRAs are configured as E-plane arrays and the other two as H-plane arrays. Each array consists of two radiating elements, evenly spaced apart. Direct microstrip line (DML) feeding, a novel kind of feeding technique to cope up with back radiation issue which occurs owing to discrete grooves on ground plane is employed to feed RDRA. The orthogonal mode in individual arrays (H-plane and E-plane) results in increased isolation. The overall dimension of the suggested quad port MIMO antenna is $(2.21\lambda_0 \times 1.32\lambda_0)$. The prescribed RDRA array operates at 5.9 GHz with an impedance bandwidth of 6.9% for Port1 and 8.1% for Port2, respectively. The measured isolation is more than -24 dB. For this MIMO antenna measured peak gain of 9.6 dBi is noticed. Various MIMO performance metrics such as the total active reflection coefficient (TARC), diversity gain (DG), channel capacity loss (CCL), and envelope correlation coefficient (ECC) have been studied in detail and discussed in this article. It is noteworthy that these measurements continue to fall within allowable threshold ranges, indicating the appropriateness of the prescribed MIMO antenna for the intended applications in intelligent automotive system.

1. INTRODUCTION

In the present decade, it is quite impossible to sustain our lives without modern wireless communications. Today's modern wireless communication demands real time and high-speed data transfer [1]. Multi-input multi-output (MIMO) is an efficient solution for these requirements where multiple antennas are used. Multiple antennas at the transmitter and receiver allow for more degrees of freedom in terms of channel capacity or system throughput. The employment of several antennas at transmitter and receiver also alleviates multipath fading in a richly scattered environment. Microstrip based MIMO antennas [2–5] have been a popular choice for the research community for the past few decades owing to their low-profile characteristics. Though patch-based MIMO antenna systems are very good candidates in low frequency applications, they suffer from severe conductor loss in high frequency applications, which restricts their usage. To mitigate this issue, a radiator made of ceramic that has appealing properties is introduced as an alternate candidate. Dielectric resonator antennas (DRAs) have a number of benefits, including being light, having a wide impedance bandwidth, having a high gain, not having any conductor loss, and being simple to excite [6, 7]. DRAs have greater degrees of design freedom because of their versatility shape. All those advantages attract researchers to work on dielectric resonator antenna (DRA) based MIMO antennas [8–13].

The intensive growth of the transportation industry leads to heavy traffic, which creates a need for an effective transportation management system. One of the best ways to alleviate this snag is intelligent transportation system (ITS). ITS is an advanced system of sensors, processing and communication technologies to improve traffic management, safety, and other factors in the transportation systems. Nowadays parking, tolling, and transportation communications employ ITS. With ITS, vehicles may communicate with infrastructure via Vehicle-to-Infrastructure (V2I) and with other vehicles through Vehicle-to-Vehicle (V2V) communication systems. One of the vital components of this ITS wireless communication is antenna. Several studies have been carried out by researchers to design antennas for intelligent vehicular systems [14, 15]. As a con-

* Corresponding author: Goffar Ali Sarkar (goffar.ali@gmail.com).

sequence of the intensive demand for high data rates and low latency in V2V communication, antenna engineers give attention to MIMO antennas for vehicular communications. In [16], two elements ultra-wideband MIMO antenna has been demonstrated using a printed monopole antenna for automotive applications. A high gain super wideband antenna with fractal loading has been employed to design MIMO antenna configuration in [17]. Metal coating is used in [18] to design a compact and multiband DRA based MIMO antenna for automobile applications. In [19], a metamaterial inspired MIMO DRA has been demonstrated with high isolation. The isolation is achieved by using a metasurface module. The authors have presented a two elements MIMO DRA for ITS applications in [20], and isolation is achieved by using the orthogonal orientation of antenna elements.

The ongoing growth of the modern automobiles furnishes luxury and safety to drivers using infotainment and automated driving assistance systems. For those features Vehicle to Everything (V2X) communication has been imparted in automobiles, which provides real time traffic information and safer driving through direct interaction with other vehicles. In this scenario, a high gain array-based MIMO antenna is necessary to mitigate path losses due to environmental and structural issues because a single antenna-based MIMO system is never adequate. So far, very few works have been published on DRA array-based MIMO antennas [21–25]. In [21–23], Hussain et al. discussed a DRA array-based MIMO antenna at millimeter wave frequency. They have used an aperture type feeding network which could result an increase in unwanted back radiation. It is also crucial to keep in mind that the planned feed network may result in undesirable phase and magnitude errors which will produce unwanted beam tilting that leads to increased antenna correlation from the expected value. The authors have investigated a filtering DRA array-based MIMO antenna in [24]. In this design, rectangular slots are used to couple the energy from the feed network. These slots may give back radiation. Additionally, the arrays are spatially separated, which poses a significant challenge for designing compact devices. In [25], a two-element array based two port MIMO antenna has been studied. S-shaped slots have been etched out on the ground plane for coupling power from the feeding line to DRA, which may lower the front to back ratio (FBR) of the antenna system. On account of spatial orientation in MIMO configuration, it also restricts the design of compact system design.

To cope up with these back radiation issues, direct microstrip line (DML) feeding to DRA is the best solution owing to its continuous ground plane. The detailed literature reviews as discussed above show that so far no one has investigated DML feed DRA array-based MIMO antennas. In this article, we introduce a novel DML fed rectangular dielectric resonator antenna (RDRA) array-based MIMO antenna operating at 5.9 GHz, mainly dedicated to ITS applications. Two radiating elements are used in each array, resulting in a peak gain of 9.6 dBi. The utilization of a continuous ground plane is the reason for our design's better gain than [22] and [23]. FBR is enhanced by this continuous ground plane as opposed to designs that have ground plane grooves. In this proposed design, we have tackled isolation by orthogonal mode excitation using H-plane and E-plane antenna arrays. The MIMO antenna has a relatively small overall footprint owing to the use of both the H- and E-plane arrays, despite an orthogonal arrangement with only E- or H-plane arrays. The overall dimension of this quad port MIMO antenna is $(2.21\lambda_0 \times 1.32\lambda_0)$. Throughout the whole working band, isolation exceeds -24 dB. The impedance bandwidth is noticed as 6.9% for Port1 and 8.1% for Port2, respectively. Additionally, the investigation on MIMO metrics (ECC, DG, CCL, and TARC) amplifies the innovative aspects of the proposed design.

2. DESIGN OF TWO ELEMENTS *H*-PLANE/*E*-PLANE ARRAYS

In this section, we develop two types of two element RDRA arrays: one configured as an H-plane array and the other as an E-plane array, as depicted in Figures 1(a) and 1(b), respectively. We have employed a traditional corporate type DML feed network [26]. Both of these arrays have been designed using a substrate (Arlon AD270) that is characterized by a relative permittivity of 2.7. Eccostock HIK material with a dielectric constant of 20 has been used to make the RDRAs, which has a height of 5.3 mm. The RDRAs are placed above the substrate in line of sight (LOS) by a separation (center to center) of $0.51\lambda_0$, where λ_0 is the free space wavelength at the operating frequency. As seen in Figure 4, the feeding networks were arranged in such a way that individual array (E-plane and H-plane) was excited orthogonally. The complete set of dimensions for the array elements has been systematically compiled and is presented in its entirety within Table 1 for easy reference and analysis.

TABLE 1. Geometrical attributes of H-plane and E-plane RDRA arrays.

Parameters	Value (mm)	Parameters	Value (mm)
L_e	67.5	L_5	17.83
L_0	2.75	L_6	8.84
L_1	6	W_e	45
L_2	4.04	W_1	1.83
L_3	8.07	W_2	1
L_4	11.815	$A = B$	9.9

The RDRAs are excited with their fundamental $TE_{111}^{X/Y}$ mode, i.e., for the H-plane array TE_{111}^{Y} mode, and that for E-plane TE_{111}^{X} is excited. The electric field distribution for the H-plane array is presented in Figure 2(a), and that for E-plane array is shown in Figure 2(b). This confirms the orthogonality of the modes for both the arrays. The simulated return losses for both the array elements are portrayed in Figure 2(c). The return loss deeps for H-plane and E-plane array elements are -15.1 dB and -22 dB at 5.9 GHz with fractional bandwidths of 7.12% and 6.8%, respectively. Figures 2(d) and 2(e) depict simulated normalized radiation patterns for the H-plane and E-plane, respectively. The arrays radiate in the broad side direction and pick gain for both arrays observed as 9.45 dBi. The cross-pol levels are 23 dB below the co-polar level for both the arrays.

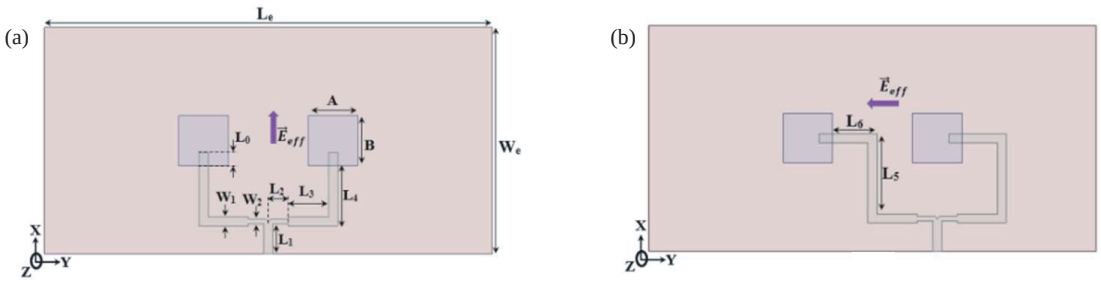

FIGURE 1. Two-element RDRA array, (a) H-plane, (b) E-plane.

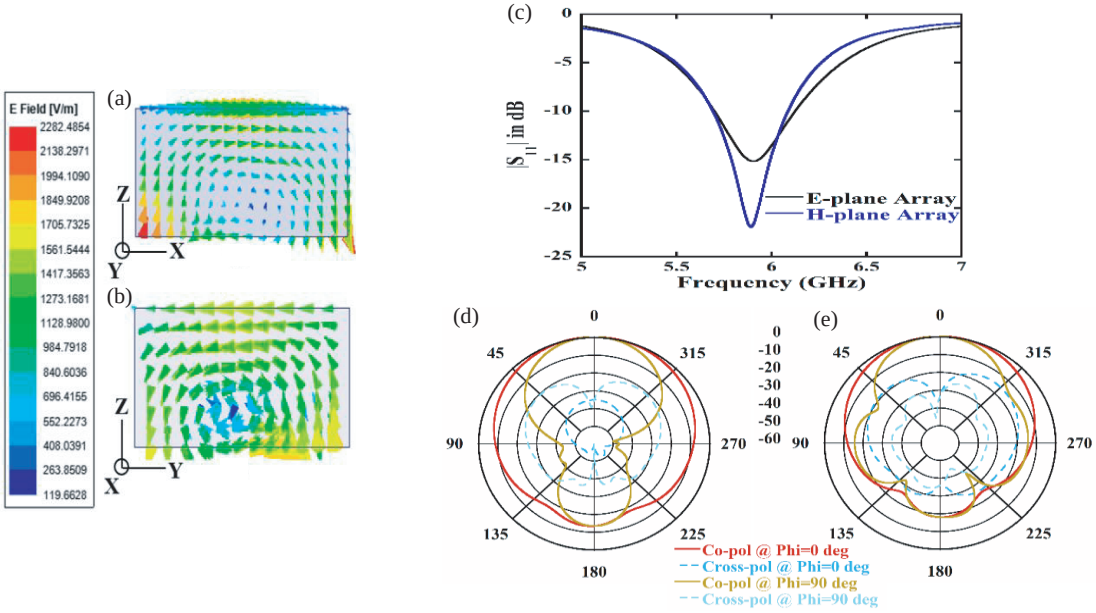

FIGURE 2. Simulated (a) electric fields for H-plane (TEs^{Y}_{111} mode), (b) electric fields for E-plane (TE^{X}_{111} mode) array, (c) S-parameters, (d) radiation patterns for H-plane Array, (e) radiation patterns for E-plane Array.

3. QUAD PORT MIMO ANTENNA CONFIGURATION

3.1. Antenna Geometry

The antenna arrays, as outlined in Section 2, served as the basis for the development of the four-port MIMO antenna. The design of MIMO antennas is a very challenging task in terms of isolation [9], while considering space constraints for compact devices. Defected ground structure (DGS), neutralization, electromagnetic band gap (EBG), and metamaterials have all been used in the literature [27–31] to enhance the isolation among the ports of the MIMO antennas. In the above-mentioned literatures, an extra circuitry is required along with the radiator, which increases the system's complexity. However, two well-known methods exist where no extra circuitry is required for isolation improvement: (i) orthogonal mode excitation [16] and (ii) exciting 180° out of phase magnetic fields [9, 10]. Owing to the orthogonal nature of the modes within the individual RDRA arrays, both in the E-plane and H-plane configurations, the arrangements depicted in Figure 3 lead to an effectively orthogonal alignment of the array elements in the MIMO antenna system. This orthogonal alignment serves to enhance the isolation between the individual elements, which is advantageous for MIMO system performance. The key design attributes and technical specifications for this MIMO antenna have been concisely presented in Table 2. The effective electric fields ($\vec{E}_{eff}$) direction of the array elements in MIMO configuration is shown by purple colour arrows which are orthogonal to each other.

To justify our mentioned comment that the effective electric fields are orthogonal to each other in the proposed MIMO configuration, we have studied the electric fields of H-plane and E-plane arrays, respectively, which are presented in Figures 4(a) and 4(b), respectively. The H-plane array's effective electric field direction is towards the X-direction whereas that for the E-plane array is in the Y-direction, i.e., the effective electric fields in the two arrays are in orthogonal to each other. Hence, arranging these arrays in MIMO configuration as in Figure 3 leads to high isolation between two adjacent ports.

3.2. Antenna Prototype and Measurement Results

To comprehensively evaluate the MIMO antenna structure, the entirety of its design was subjected to simulation using Ansys HFSS 19 software. To corroborate the accuracy and consistency of the simulated outcomes, a physical prototype was

TABLE 2. Design parameters of DRA array based MIMO antenna configuration.

Parameters	Value (mm)	Parameters	Value (mm)
L	112.5	W	67.5
L_0	2.75	W_1	1.83
L_1	6	W_2	1
L_2	4.04	$A = B$	9.9
L_3	8.07	D	16.15
L_4	11.815	H	5.3
L_5	17.83	h	0.79
L_6	8.84	-	-

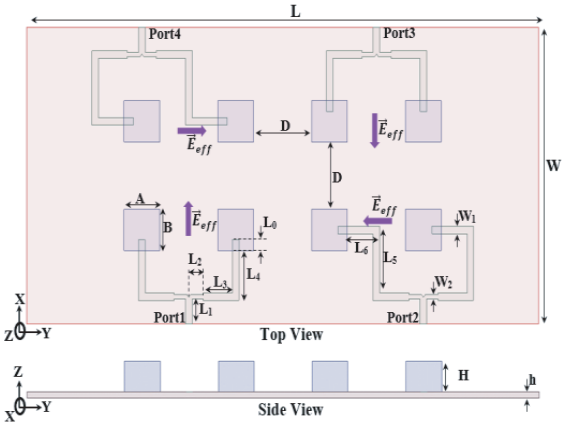

FIGURE 3. Schematic view of RDRA Array based Quad Port MIMO Antenna configuration.

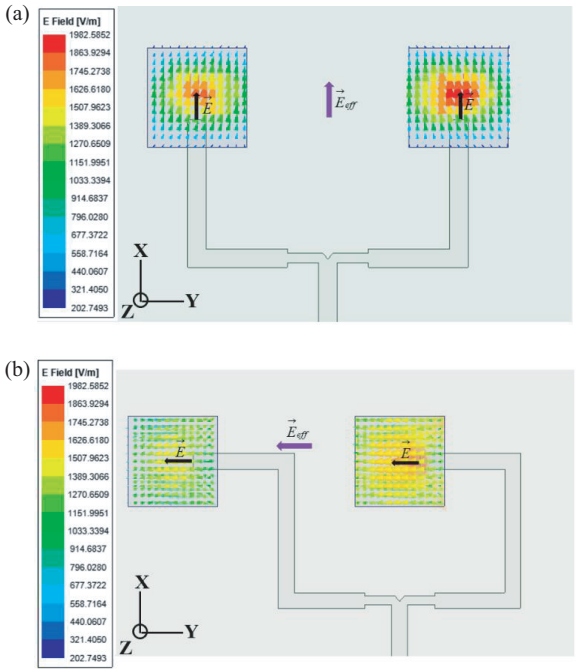

FIGURE 4. Electric fields, (a) H-plane, (b) E-plane array.

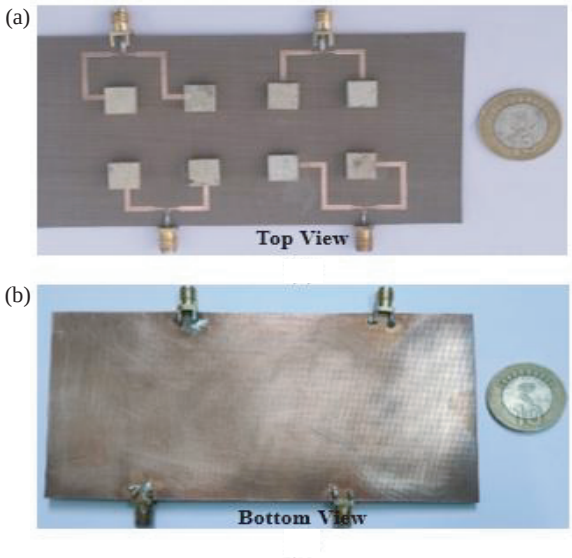

FIGURE 5. (a) Top View of the Quad Port MIMO, (b) Bottom View of the Quad Port MIMO antenna.

meticulously constructed utilizing an Arlon AD270 substrate. Figure 5(a) clearly presents top view of the prototype. Figure 5(b) illustrates the antenna's back side and confirms the existence of a continuous ground plane. This continuous ground plane is a critical component of the antenna's design and functionality. S-parameters of the antenna are measured using VNA by Anritsu (S820E), and measured results are depicted along with the simulated ones in Figures 6(a) and 6(b). Only six (S_{11}, S_{22}, S_{21}, S_{31}, S_{41}, S_{42}) parameters are shown instead of sixteen parameters due to the symmetrical arrangement of the arrays in MIMO configuration. There is a clear similarity between the measured and simulated findings. The fact that the expected and actual results line up highlights how accurate and dependable the model or experiment is. The deeps of the reflection coefficients occur at 5.9 GHz with impedance bandwidths of 6.9% for Port1 and 8.1% for Port2, respectively.

Normalized radiation patterns of the array-based MIMO antenna are studied for Port1 and Port2, keeping all other ports (except the excited one) terminated with 50 Ω matched load at both the planes-$\phi = 0°$ and $\phi = 90°$. The radiation patterns are depicted in Figures 6(c)–6(f). The measured results closely resemble the simulated ones. For both ports, peak gain is measured as 9.6 dBi. 3 dB beamwidths for Port1 are measured as $\pm 45°$ and $\pm 22°$ for $\phi = 0°$ and $\phi = 90°$ planes, respectively, whereas those for Port2 are $\pm 38°$ and $\pm 17°$ for $\phi = 0°$ and $\phi = 90°$ planes, respectively. The cross-polarization levels are more than 20 dB below the co-polarization level which is quite acceptable.

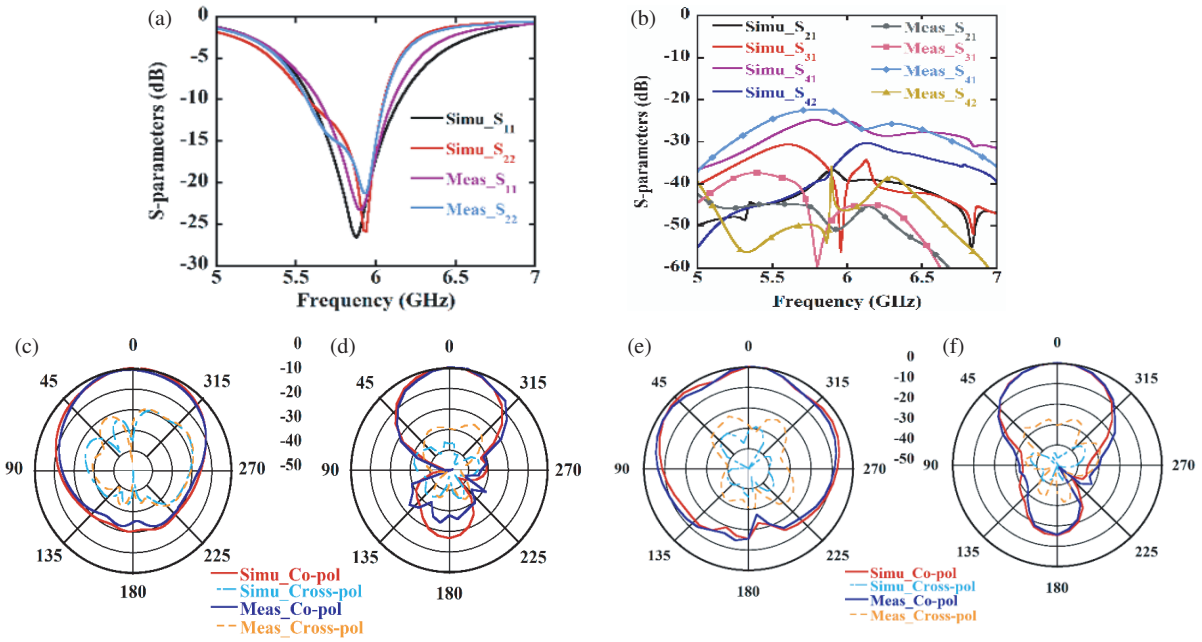

FIGURE 6. Simulated and practically observed, (a) Reflection Coefficients, (b) Isolation, (c) Radiation patterns for Port1 @ $\phi = 0°$, (d) Radiation patterns for Port1 @ $\phi = 90°$, (e) Radiation patterns for Port2 @ $\phi = 0°$, (f) Radiation patterns for Port2 @ $\phi = 90°$.

3.3. Diversity Performance

The performance of the MIMO antenna cannot be appraised by only studying isolation. Moreover, we need to address a few important MIMO metrics like ECC, DG, CCL, total TARC, etc. ECC is one of the most vital parameters that need to be studied in MIMO antenna systems. It reveals how much two antennas are correlated. It is an obvious desire to have highly uncorrelated antennas in the MIMO system. The ECC parameter can be calculated by far field radiation patterns using (1) [9]:

$$\rho_e = \frac{\left| \iint\limits_{4\pi} \left[\overrightarrow{F_1}(\theta,\phi) * \overrightarrow{F_2}(\theta,\phi) \right] d\Omega \right|^2}{\iint\limits_{4\pi} \left| \overrightarrow{F_1}(\theta,\phi) \right|^2 d\Omega \iint\limits_{4\pi} \left| \overrightarrow{F_2}(\theta,\phi) \right|^2 d\Omega} \tag{1}$$

where $\overrightarrow{F_1}(\theta,\phi)$ is the far-field 3D pattern of the antenna when ith port is excited, Ω the solid angle, and $(*)$ the Hermitian product operator. The calculation of ECC taking far-field patterns is very tedious and time consuming, hence in highly efficient (efficiency $> 90\%$) MIMO antenna, ECC is determined using S-parameters as (2) [9]:

$$\rho_e = \frac{\left| S_{11}^* S_{12} + S_{21}^* S_{22} \right|^2}{\left(1 - |S_{11}|^2 - |S_{21}|^2\right)\left(1 - |S_{12}|^2 - |S_{22}|^2\right)} \tag{2}$$

where S_{ii} represents the return loss coefficients, and S_{ij} represents the isolation between the ith and jth ports. This MIMO antenna possesses efficiency more than 95%. Hence, in this article, we have used the S-parameters to evaluate the measured as well as simulated ECC of this proposed DRA array-based MIMO antenna, and the findings are graphically represented in Figure 7(a). It has been noticed that the ECC is < 0.002 throughout the operating band which is much less than the diversity thumb value of 0.5 [9]. The diversity gain (DG) is another crucial parameter that resembles the improvement of signal to interference and is computed utilizing (3) [9]:

$$DG = 10\sqrt{1 - |\rho_e|^2} \tag{3}$$

where ρ_e is the ECC. The calculated DG is delineated in Figure 7(b). Enhancing channel capacity is one of the primary objectives in the development and deployment of MIMO antenna technology. Channel capacity is influenced not only by the number of antennas utilized but also by the correlation among those antennas. Greater inter-antenna correlation results in an increased loss of channel capacity, which is quantified in bits per second per hertz (bits/s/Hz). Hence, it is highly desirable to make sure that antennas are highly uncorrelated in MIMO configurations. CCL is calculated using (4)–(7) [9]:

$$C_{loss} = -\log_2 \det(\Psi^R) \tag{4}$$

where,

$$\Psi^R = \begin{bmatrix} \Psi_{11} & \Psi_{12} & \Psi_{13} & \Psi_{14} \\ \Psi_{21} & \Psi_{22} & \Psi_{23} & \Psi_{24} \\ \Psi_{31} & \Psi_{32} & \Psi_{33} & \Psi_{34} \\ \Psi_{41} & \Psi_{42} & \Psi_{43} & \Psi_{44} \end{bmatrix} \tag{5}$$

$$\Psi_{ii} = 1 - \left(\sum\nolimits_{n=1}^{4} |S_{in}^* S_{ni}| \right) \tag{6}$$

$$\Psi_{ij} = - \left(\sum\nolimits_{n=1}^{4} |S_{in}^* S_{nj}| \right)$$

$$\text{where, } i, j = 1, 2, 3, 4 \text{ and } i \neq j. \tag{7}$$

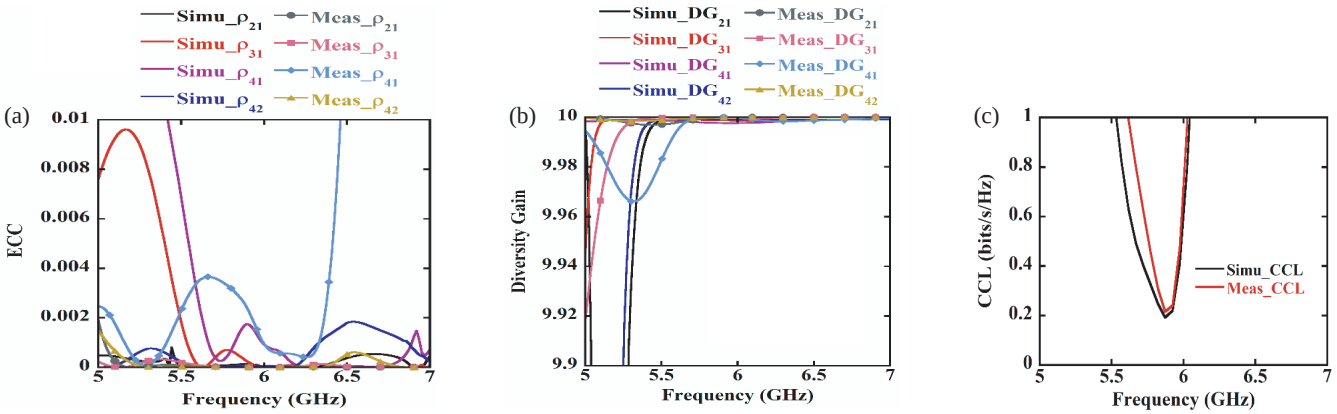

FIGURE 7. Simulated and practically observed, (a) ECC, (b) Diversity Gain, (c) CCL.

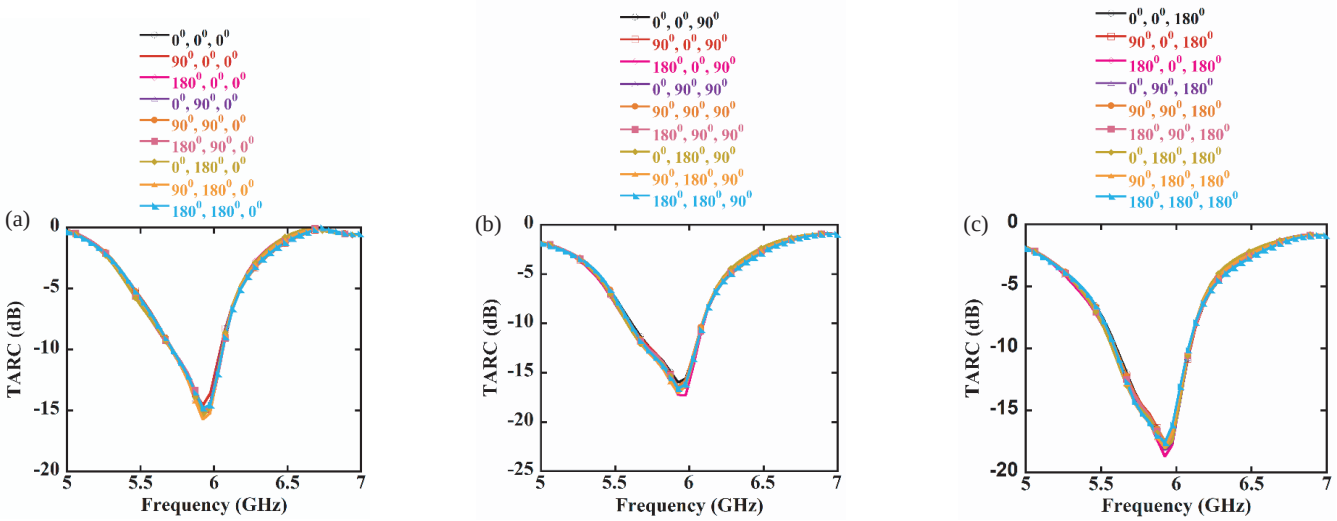

FIGURE 8. (a)–(c) Variations in the TARC value across different combinations of phase angles.

Figure 7(c) showcases the computed CCL derived from both measured and simulated data. It is evident from the plot that the CCL is well below its prescribed practical value (0.4 bits/s/Hz). The dissimilarity between the results mights be attributed to the manual positioning of the dielectric resonator (DR) on top of the substrate, as well as the use of glue to attach the DR to the substrate. Even if the simulated and measured results differ somewhat, the diversity parameters' values stay under the threshold range and provide an acceptable level of performance within the working band.

The determination of impedance bandwidth in MIMO antenna systems cannot solely rely on the reflection coefficient, as it necessitates consideration of additional factors and parameters to provide a comprehensive assessment. Another important performance parameter TARC needs to be addressed for calculating active operating bandwidth. TARC is calculated from S-parameters by (8)–(10) [24]:

$$\Gamma_a^t = \frac{\sum_{n=1}^{N} |b_i|^2}{\sum_{n=1}^{N} |a_i|^2} \tag{8}$$

$$[b] = [S]\,[a] \tag{9}$$

$$\begin{bmatrix} b_1 \\ b_2 \\ b_3 \\ b_4 \end{bmatrix} = \begin{bmatrix} S_{11} & S_{21} & S_{31} & S_{41} \\ S_{12} & S_{22} & S_{32} & S_{42} \\ S_{13} & S_{23} & S_{33} & S_{43} \\ S_{14} & S_{24} & S_{34} & S_{44} \end{bmatrix} \begin{bmatrix} a_1 \\ a_2 \\ a_3 \\ a_4 \end{bmatrix} \tag{10}$$

where a_i and b_i are incident and reflected waves, respectively. $[a]$, $[b]$, and $[S]$ stand for incident matrix, reflected matrix, and S-parameter matrix, respectively. For different excited phase combinations of Port2, Port3, and Port4, TARC is presented in Figures 8(a)–8(c) while keeping Port1 excitation to 0° (if the legend is given as 90°, 180°, 90° which means that Port2, Port3, Port4 are excited with a phase shift of 90°, 180°, and 90°, respectively). Analysis of the figures, specifically denoted as Figure 8, clearly illustrates that the TARC remains consistently below the -10 dB threshold throughout the designated operating frequency band, substantiating the antenna's performance characteristics.

TABLE 3. Comparative analysis between the proposed work and previously reported studies.

Ref.	DRA Shape	Isolation Technique	Isolation (dB)	ECC	DG	TARC	Antenna Footprint	Gain (dBi)	Array MIMO	Distance Between Antenna Elements	Number ports
[12]	Hut-DRA	Orthogonal and Discrete Ground Plane	-20	-	≈ 10	Not addressed	$1.35\lambda_0 \times 1.35\lambda_0$	4.0	N	-	4
[13]	RDRA	Small Secondary DiscreteGround Plane	-30	-	-	Not addressed	$2.91\lambda_0 \times 1.4\lambda_0$	13.2	N	$0.5\lambda_0$	4
[21]	CRDA	Beam tilting	-20	0.01	-	Not addressed	$5\lambda_0 \times 2\lambda_0$	9	Y	$0.6\lambda_0$	2
[22]	CRDA	Beam tilting	-15	0.02	-	Not addressed	$7.2\lambda_0 \times 3.9\lambda_0$	10	Y	$0.6\lambda_0$	4
[23]	CRDA	Beam tilting	-15	0.002	-	Not addressed	$4.8\lambda_0 \times 2.1\lambda_0$	10	Y	$0.6\lambda_0$	2
[24]	RDRA	Space between MIMO elements	-17	0.01	> 9.99	Addressed	$1.12\lambda_0 \times 0.84\lambda_0$	7.8	Y	$0.53\lambda_0$	2
[25]	HDRA	Space between MIMO elements	-25	0.05	> 9.99	Addressed	$2.54\lambda_0 \times 0.6\lambda_0$	9.2	Y	$0.48\lambda_0$	2
This Work	**RDRA**	**Orthogonality is** achieved by arranging E-plane and H-plane array	**-24**	**0.002**	**> 9.99**	**Addressed**	**$2.21\lambda_0 \times 1.32\lambda_0$**	**9.6**	**Y**	**$0.31\lambda_0$**	**4**

3.4. Performance Comparison

The proposed array-based MIMO antenna is compared with other existing works in Table 3. This array arrangement in MIMO provides a sound isolation without any extra circuitry (worse case: -24 dB) which highlights the novelty of this work. The proposed design gives better ECC and DG responses than others works. Though this work appears to have a larger footprint than [24, 25], the suggested design exhibits superior performance in the context of MIMO capabilities such as ECC and number of ports (this design has quad ports whereas [24, 25] have two ports i.e., our proposed design has a greater number of ports than [24, 25]). It can be inferred from Table 3 that the array based MIMO antennas as presented in [22] and [23] have lager gain than the proposed work which can be attributed to the number of array elements used in each array. In [22] and [23], four elements have been used in each array while in this works the authors have used two elements. It is obvious that a greater number of elements in an array may give more gain. The design also provides more gain than the works presented in [24] and [25]. The proposed design has the lowest elemental distance in terms of free space wavelength despite their elevated isolation. It can be inferred from Table 3 that our proposed designs have significant and sound innovation.

4. CONCLUSION

A simply designed RDRA array-based MIMO antenna with quad ports is described and tested for 5.9 GHz operation which is dedicated to Intelligent Transportation System applications. The proposed quad-port MIMO design comprises two E-plane arrays and two H-plane arrays. This configuration enhances the system's capabilities for MIMO communication. While using in MIMO configuration, the arrays are arranged in such a way so that they effectively provide orthogonal layouts, which leads to high port isolation. The MIMO antenna has impedance bandwidths of 6.9% and 8.1% for Port1 and Port2, respectively. It yields 9.6 dBi peak gain with considerably low cross polarization level. MIMO performance metrics of this MIMO antenna are found to be under the thumb value. Hence, we can comment that the suggested design would be a good fit for ITS band applications.

REFERENCES

[1] Singhwal, S. S., B. K. Kanaujia, A. Singh, J. Kishor, and L. Matekovits, "Dual-band circularly polarized MIMO DRA for sub-6 GHz applications," *International Journal of RF and Microwave Computer-Aided Engineering*, Vol. 30, No. 10, e22350, 2020.

[2] Mandloi, M. S., P. Gupta, A. Parmar, P. Malviya, and L. Malviya, "Beamforming MIMO array antenna for 5G-millimeter-wave application," *Wireless Personal Communications*, Vol. 129, No. 1, 153–172, 2023.

[3] Kaur, I., M. Bareilly, B. Basu, and A. Singh, "Sub-6 GHz metallic via integrated MIMO antenna array for 5G smartphone," *Progress In Electromagnetics Research C*, Vol. 138, 91–104, 2023.

[4] Kiani, S. H., H. S. Savci, H. S. Abubakar, N. O. Parchin, H. Rimli, and B. Hakim, "Eight element MIMO antenna array with tri-band response for modern smartphones," *IEEE Access*,

Vol. 11, 44 244–44 253, 2023.

[5] Su, J., B. Lin, H. Dou, and X. Chen, "A freely extendable closely packed dual-band MIMO antenna for 5G wireless communication," *Progress In Electromagnetics Research Letters*, Vol. 114, 21–29, 2023.

[6] Rana, B. and S. K. Parui, "Nonresonant microstrip patch-fed dielectric resonator antenna array," *IEEE Antennas and Wireless Propagation Letters*, Vol. 14, 747–750, 2014.

[7] Petosa, A., *Dielectric Resonator Antenna Handbook*, Artech House, 2007.

[8] Sahu, N. K. and R. K. Gangwar, "Dual-port compact MIMO-DRAs: Exploiting metallic sheets to increase inter-port isolation at 28-GHz 5G-band," *IEEE Transactions on Circuits and Systems II: Express Briefs*, Vol. 69, No. 12, 4814–4818, 2022.

[9] Sarkar, G. A., S. Ballav, A. Chatterjee, S. Ranjit, and S. K. Parui, "Four element MIMO DRA with high isolation for WLAN applications," *Progress In Electromagnetics Research Letters*, Vol. 84, 99–106, 2019.

[10] Sarkar, G. A. and S. K. Parui, "A two element MIMO dielectric resonator antenna for WLAN application," in *2018 IEEE MTT-S International Microwave and RF Conference (IMaRC)*, 1–3, 2018.

[11] Zhang, B., J. Ren, T. Yang, Y.-T. Liu, Z. Zhao, J. Zhao, Y. Liu, and Y. Yin, "Three-port pattern-and polarization-diversity rectangular dielectric resonator antenna," *IEEE Transactions on Antennas and Propagation*, Vol. 71, No. 6, 5392–5397, 2023.

[12] Tyagi, K., A. K. Dwivedi, S. K. Singh, P. Ranjan, and A. Sharma, "Four port dielectric resonator based MIMO antenna design for cognitive radio applications," *IEEE Transactions on Circuits and Systems II: Express Briefs*, Vol. 70, No. 6, 1936–1940, 2022.

[13] Song, S., X. Chen, Y. Da, and A. A. Kishk, "Broadband dielectric resonator antenna array with enhancement of isolation and front-to-back ratio for MIMO application," *IEEE Antennas and Wireless Propagation Letters*, Vol. 21, No. 7, 1487–1491, 2022.

[14] Zhang, Y., J.-Y. Deng, D. Sun, J.-Y. Yin, and L.-X. Guo, "Compact slow-wave SIW H-plane horn antenna with increased gain for vehicular millimeter wave communication," *IEEE Transactions on Vehicular Technology*, Vol. 70, No. 7, 7289–7293, 2021.

[15] Xia, Z.-X., K. W. Leung, P. Gu, and R. Chen, "3-D-printed wideband high-efficiency dual-frequency antenna for vehicular communications," *IEEE Transactions on Vehicular Technology*, Vol. 71, No. 4, 3457–3469, 2022.

[16] Alsath, M. G. N. and M. Kanagasabai, "Compact UWB monopole antenna for automotive communications," *IEEE Transactions on Antennas and Propagation*, Vol. 63, No. 9, 4204–4208, 2015.

[17] Prabhu, P. and S. Malarvizhi, "Koch fractal loaded high gain super-wideband diversity THz MIMO antenna for vehicular communication," *Optical and Quantum Electronics*, Vol. 54, No. 11, 726, 2022.

[18] Chiu, T.-L., L. Huitema, O. Pajona, and T. Monediere, "Compact and multiband MIMO dielectric resonator antenna for automotive LTE communications," *International Journal of Antennas and Propagation*, 1–15, 2018.

[19] Dwivedi, A. K., A. Sharma, A. K. Singh, and V. Singh, "Metamaterial inspired dielectric resonator MIMO antenna for isolation enhancement and linear to circular polarization of waves," *Measurement*, Vol. 182, 109681, 2021.

[20] Sarkar, G. A., S. K. Parui, and S. Banerjee, "A dielectric resonator MIMO antenna for intelligent transportation systems," in *Advances in Smart Communication Technology and Information Processing: Optronix 2020*, 3–9, 2021.

[21] Hussain, M. T., O. Hammi, M. S. Sharawi, S. K. Podilchak, and Y. M. M. Antar, "A dielectric resonator based millimeter-wave MIMO antenna array for hand-held devices," in *2015 IEEE International Symposium on Antennas and Propagation & USNC/URSI National Radio Science Meeting*, 3–4, 2015.

[22] Hussain, M. T., M. S. Sharawi, S. Podilchack, and Y. M. M. Antar, "Closely packed millimeter-wave MIMO antenna arrays with dielectric resonator elements," in *2016 10th European Conference on Antennas and Propagation (EuCAP)*, 1–4, 2016.

[23] Sharawi, M. S., S. K. Podilchak, M. T. Hussain, and Y. M. M. Antar, "Dielectric resonator based MIMO antenna system enabling millimetre-wave mobile devices," *IET Microwaves, Antennas & Propagation*, Vol. 11, No. 2, 287–293, 2017.

[24] Ballav, S., G. A. Sarkar, and S. K. Parui, "Filtering DRA array and its applications in MIMO for sub-6 GHz band," *Radioengineering*, Vol. 30, No. 1, 73–80, 2021.

[25] El-Nady, S. M., A. S. A. El-Hameed, E. M. Eldesouki, and S. A. M. Soliman, "Circularly polarized MIMO filtering dielectric resonator antenna for 5G sub-6 GHz applications," *AEU-International Journal of Electronics and Communications*, Vol. 171, 154882, 2023.

[26] Sarkar, G. A., B. Rana, and S. K. Parui, "A direct microstrip line feed hemispherical dielectric resonator antenna array," in *2017 1st International Conference on Electronics, Materials Engineering and Nano-technology (IEMENTech)*, 1–3, 2017.

[27] Niu, Z., H. Zhang, Q. Chen, and T. Zhong, "Isolation enhancement for 1×3 closely spaced E-plane patch antenna array using defect ground structure and metal-vias," *IEEE Access*, Vol. 7, 119 375–119 383, 2019.

[28] Tiwari, R. N., P. Singh, and B. K. Kanaujia, "A compact UWB MIMO antenna with neutralization line for WLAN/ISM/mobile applications," *International Journal of RF and Microwave Computer-Aided Engineering*, Vol. 29, No. 11, e21907, 2019.

[29] Beigi, P., M. Rezvani, Y. Zehforoosh, J. Nourinia, and B. Heydarpanah, "A tiny EBG-based structure multiband MIMO antenna with high isolation for LTE/WLAN and C/X bands applications," *International Journal of RF and Microwave Computer-Aided Engineering*, Vol. 30, No. 3, e22104, 2020.

[30] Murthy, N., "Improved isolation metamaterial inspired mm-wave MIMO dielectric resonator antenna for 5G application," *Progress In Electromagnetics Research C*, Vol. 100, 247–261, 2020.

[31] Mishra, N. K., J. Acharjee, V. Sharma, C. Tamrakar, and L. Dewangan, "Mutual coupling reduction between the cylindrical dielectric resonator antenna using split ring resonator based structure," *AEU-International Journal of Electronics and Communications*, Vol. 154, 154305, 2022.